

Fundamental and derived modes of climate variability: concept and application to interannual time-scales

By MIHAI DIMA^{1,2*} and GERRIT LOHMANN¹, ¹*Bremen University, Department of Geosciences and Research Center Ocean Margins, PO Box 330 440, D-28334 Bremen, Germany;* ²*University of Bucharest, Faculty of Physics, Department of Atmospheric Physics, PO Box MG-11, Bucharest, Romania*

(Manuscript received 3 April 2003; in final form 19 December 2003)

ABSTRACT

The notion of mode interaction is proposed as a deterministic concept for understanding climatic modes at various time-scales. This concept is based on the distinction between fundamental modes relying on their own physical mechanisms and derived modes that emerge from the interaction of two other modes. The notion is introduced and applied to interannual climate variability. Observational evidence is presented for the tropospheric biennial variability to be the result of the interaction between the annual cycle and a quasi-decadal mode originating in the Atlantic basin. Within the same framework, Pacific interannual variability at time-scales of about 4 and 6 yr is interpreted as the result of interactions between the biennial and quasi-decadal modes of climate variability. We show that the negative feedback of the interannual modes is linked to the annual cycle and the quasi-decadal mode, both originating outside the Pacific basin, whereas the strong amplitudes of interannual modes result from resonance and local positive feedback. It is argued that such a distinction between fundamental and derived modes of variability is important for understanding the underlying physics of climatic modes, with strong implications for climate predictability.

1. Introduction

Spectra of climatic time series are characterized by three important features: continuity, redness (slope towards longer time-scales in the power spectra) and presence of multiple peaks (Mitchell, 1976). The redness can be attributed to stochastic mechanisms in which random high-frequency fluctuations, e.g. weather systems, are being integrated by the much slower responding components of the climate system, e.g. the ocean (Hasselmann, 1976). Therefore, the low-frequency fluctuations develop and grow in amplitude with increasing time-scale. In this stochastic climate model concept (Hasselmann, 1976), the variance is limited by the negative feedback mechanisms within the climate system.

The clear distinction of peaks in the climate spectra suggests that deterministic processes may be responsible for their generation. For example, there is climate variability at preferred time-scales due to internal oscillations such as the El Niño Southern Oscillation (ENSO) phenomenon (Philander, 1990) or the Atlantic quasi-decadal (QD) mode (Deser and Blackmon, 1993; Dima et al. 2001), or due to external forcing such as the annual cycle or the astronomical Milankovitch cycles.

The stochastic climate model is based on its analogy with the Brownian motion, being characterized by slow and fast evolving systems within the same model (Einstein, 1905). However, climatic oscillations may be the result of deterministic processes associated with two active climate components, e.g. atmosphere–ocean interactions (Bjerknes, 1964; Latif and Barnett, 1994; Latif, 1998; Timmermann et al. 1998). Because of their decorrelation time-scale, such oscillatory modes can yield much longer predictability than is expected to emerge from the stochastic climate model.

Modes of climate variability have been identified through statistical analysis of observations and model data. For example, recent observational studies have shown that a large part of the Pacific climate variance can be attributed to ENSO or ENSO-like modes (Mantua et al. 1997) while a distinct part of the surface climate variability in the North Atlantic can be attributed to a QD mode characterized by a ‘tripole pattern’ of sea surface temperature (SST; Deser and Blackmon, 1993; Mann and Park, 1994; Zhang et al. 1997).

Two general characteristics of the climate variability emerge from the analysis of historical data. First, modes of interannual and interdecadal variability are identified and described in both the Pacific and Atlantic basins. Secondly, we can note that the patterns associated with different modes of variability share common features; for example, the Pacific modes with their

*Corresponding author.
e-mail: dima@palmod.uni-bremen.de

characteristic ENSO-like structures have strong projections onto the ‘tripole’ SST in the Atlantic basin (Zhang et al. 1997). Based on this finding, one may wonder if these modes may in fact be based on common physical processes and if these shared features are the result of a common origin for these specific climate variations.

Here we investigate the interannual to decadal variability during the observational period based on the conceptual framework of fundamental and derived modes to be described in Section 2. We apply this concept to biennial (Section 3), interannual and decadal (Section 4) climate variability. Conceptual features of the mode interaction principle are discussed in Section 5 and conclusions are drawn in Section 6.

2. Concept

A central problem in climate research is to reduce the numerous space–time degrees of freedom of the climate system to a minimum number of climatic modes that can explain a maximal part of its variability. On one hand, methods have been designed to identify dominant spatial structures, e.g. empirical orthogonal functions (EOFs), canonical correlation analysis (CCA), principal oscillation patterns (POPs) and cluster analysis (von Storch and Zwiers, 1999). One may view the spatial patterns emerging from such methods of analysis as points in the phase space where the probability density function is very high. On the other hand, different methods have been developed to identify quasi-periodic time evolutions, e.g. spectral analyses, singular spectrum analysis (SSA) and wavelet analysis (for an overview, see von Storch and Zwiers, 1999).

It is important to point out the duality of these two types of methods in the analysis of climate variability. By projecting a spatial pattern given by an analysis in the first category (EOF, CCA, POP) onto the initial data from which the spatial structure was first derived, we obtain the associated time evolution. Similarly, by regressing the quasi-periodic components derived with a time domain analysis (SSA, wavelet analysis) onto the spatial fields, we obtain the associated spatial structures. Thus, the two types of method complement each other. This space–time complementarity can also be described in analogy with the particle–wave duality. The spatial structures may be associated with the particle concept, while the quasi-periodic signals would be analogous to the wave concept (Ghil and Robertson, 2002).

An optimal correspondence is obtained when the time evolution of a dominant spatial structure is periodic. In such cases, the time evolution of a whole set of physical processes that contribute to the generation of the mode’s spatial structure is reduced to a quasi-periodic time component, therefore significantly reducing the number of degrees of freedom.

Such periodic climate modes with coherent spatial structures were identified in the tropical Pacific (Philander, 1990) and North Atlantic (Deser and Blackmon, 1993). It is conceivable that other modes are being generated through a superposition or, more gen-

erally, through an interaction between climatic modes. In this case, the problem of understanding climate variability can be reduced to the problem of identifying the basic modes and describing their interactions. Given the quasi-periodic evolution of climatic eigenmodes, the simplest approach to this problem would be to describe the interaction between the modes in the Fourier domain for their respective time components (e.g. the principal components associated with the spatial EOFs).

2.1. Superposition concept

Consider two modes with comparable amplitudes and characterized by quasi-periodic variability with periods T_1 and T_2 . The signal that results from the superposition of the time components associated with these two modes may be represented as a sum or as a product of harmonic functions according to the relation:

$$\begin{aligned} & \sin(2\pi t/T_1 + \varphi_1) + \sin(2\pi t/T_2 + \varphi_2) \\ &= 2 \sin(2\pi t/T_A + \varphi_A) \cos(2\pi t/T_B + \varphi_B). \end{aligned} \quad (1)$$

Through this transformation (going from left to right in relation 1), two new modes with periods T_A and T_B are generated. The new periods and phases are given by the relations:

$$T_A = 2T_1T_2/(T_2 + T_1) \quad (2a)$$

$$T_B = 2T_1T_2/(T_2 - T_1) \quad (2b)$$

$$\varphi_A = (\varphi_1 + \varphi_2)/2 \quad (3a)$$

$$\varphi_B = (\varphi_2 - \varphi_1)/2. \quad (3b)$$

A particular case is $T_2 \gg T_1$, when the periods of the two derived modes, T_A and T_B in eq. (2), are very close to each other and approximately equal to $2T_1$. The transformation (1) may also be applied for two modes with different amplitudes, say A_1 and A_2 , respectively, for the terms on the left-hand side in relation (1). Then A_2 may be substituted for $A_1 + (A_2 - A_1)$, and the two signals with amplitude A_1 , but distinct periods (T_1 and T_2), are transformed according to relation (1).

2.2. Selection and amplifying mechanisms

A physical representation of the relation given by eq. (1) may be constructed. Consider two modes with different origins (e.g. originating in different oceanic basins) and both influencing the atmosphere (Fig. 1). In the Fourier space, the resulting atmospheric state is described by the superposition of the two signals, the left-hand side in relation (1). A Fourier analysis performed on the resulted signal would then identify the initial time components. Furthermore, assume that the resulting signal is applied to the ocean, which would in turn transform and release the signal back into the atmosphere. The oceanic transfer function may be non-linear so that in some regions one of the harmonic components on the right-hand side of relation (1) is amplified, while

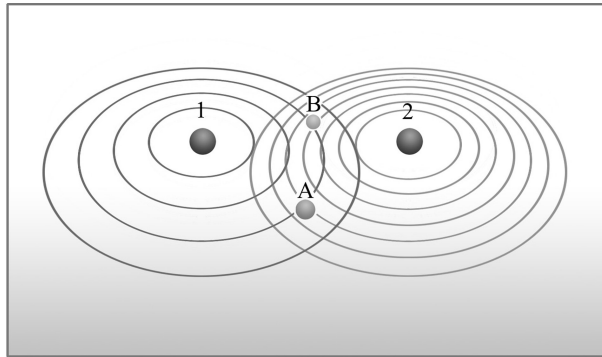


Fig 1. Schematic representation of the superposition of two climate modes.

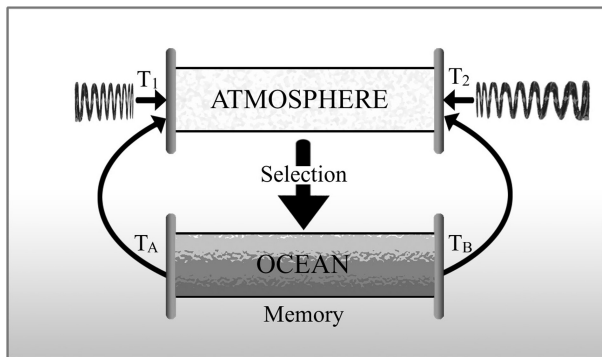


Fig 2. Schematic representation of the mode interaction concept.

in other regions the other harmonic component in the product becomes amplified. Such non-linearity may be given by the different spatial propagation of oceanic waves with various periods or by the waveguides. Therefore, we can define a selection mechanism through the physical processes with different characteristic time-scales which generate distinct spatial and/or temporal effects. Furthermore, some of the already differentiated frequencies may be significantly amplified, generally through positive feedbacks. In other words, a frequency on the right-hand side in relation (1), separated through selection mechanisms, may subsequently fall into resonant structures, and therefore the corresponding mode becomes amplified. In this way the amplitude of this mode may grow significantly larger than the amplitude of the other component on the right-hand side of eq. (1). As a result, the resonant modes appear as quasi-independent modes that can be detected in the Fourier spectrum.

A schematic representation of our concept is presented in Fig. 2. Here it is suggested that the signal resulting from two fundamental modes is non-linearly transformed (selected) by the ocean so that two new modes (derived modes) are generated. The resulting selected modes (derived modes) may be amplified by positive feedbacks associated with inherent growing climate modes.

To exemplify, we consider climate variations in the tropical Pacific ocean where spatial structures linked to the Rossby and Kelvin waveguides provide a pool of resonant structures with specific time periods (Gill, 1982). Waves with characteristic periods can propagate optimally in some regions, while waves with other periods are damped in the same areas. This property of the ocean may be regarded as a differential spatial resonance between atmospheric and oceanic modes and we refer to it as ‘selection’. If the ocean is forced by an atmospheric signal which may be represented as a product of two periodic components, due to its ‘selective’ property and to possible positive feedback involved, it may amplify one of the two components in some regions, while the other component is amplified in different regions. Therefore, through the selection process, the two components which initially were part of the product (the right-hand side of relation 1), appear as quasi-independent signals.

Figure 3 presents an example for such ‘selection’. The figure shows the first modes obtained from two EOF analyses on the SST fields (Kaplan et al. 1998), for the 1856–2000 periods. In both cases, the anomalous fields were first detrended. In the first EOF analysis, only time-scales in the biennial band were retained, while in the second analysis only time-scales in the bidecadal band were retained. The main difference between the two EOFs is the latitudinal extensions of SST anomalies which is most likely due to the differential propagation of planetary waves (Moore et al. 1978; Gill, 1982; Killworth et al. 1997; Tourre et al. 2001). Such wave differential propagation can be then considered a spatial selection mechanism.

Distinct from this, a spatio-temporal selection mechanism is represented by the concept of rectification (Milankovitch, 1941; Clement et al. 1999; Huybers and Wunsch, 2003). Rectification may be viewed as the transformation through which a low-frequency signal only modulates one phase (for example, the positive phase) of a high-frequency component. A physical analogy to the tropical Pacific variability may be constructed if one considers the meridional movement of the Walker Cell, which is modulated by a product term like the one on the right-hand side of eq. (1), a product of 8- and 20-yr signals. We assume that the relatively high-frequency signal (e.g. the 8-yr mode) influences the meridional movement of the Walker circulation. Then, at a given point not far from equator, the direct Walker Cell influence would be felt only during given phases of the 8-yr components. Therefore, the bidecadal component, as the modulating frequency, is detected by Fourier analysis due to the rectification of the 8-yr mode. To summarize, it is argued that the derived modes of variability are being generated by specific selecting and amplifying mechanisms.

2.3. Fundamental versus derived modes

One may wonder about what causes an internal mode of variability to be considered a fundamental mode? We argue that there are two elements necessary for the generation of oscillatory internal

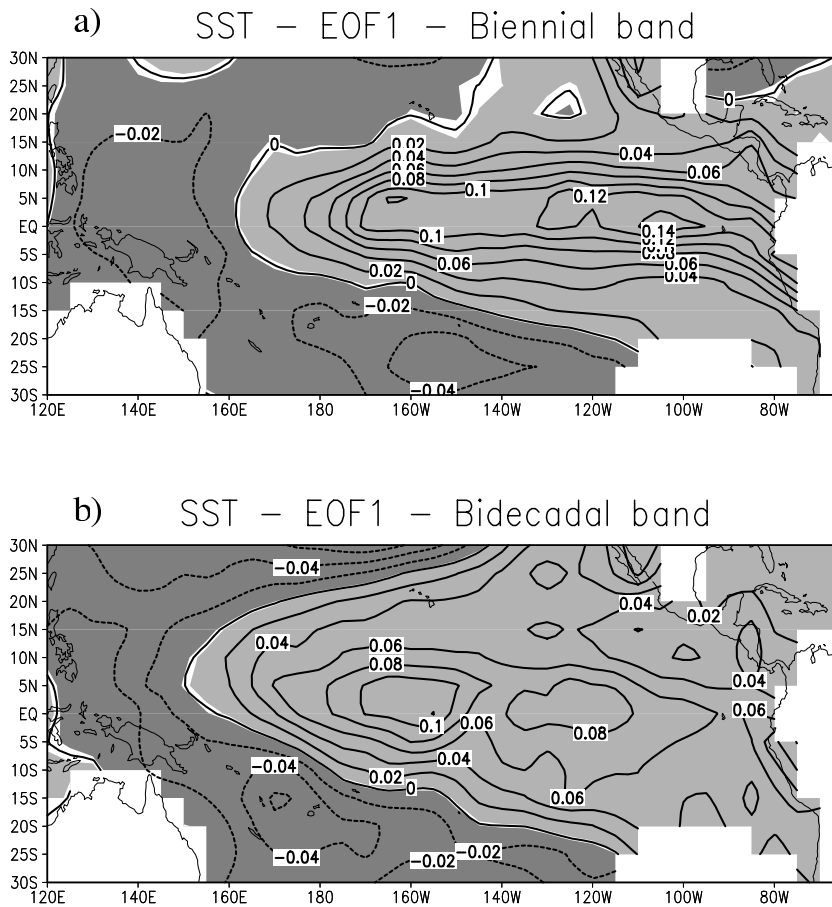


Fig 3. The first EOFs calculated from the SST data set (Kaplan et al. 1998) over the 1856–2000 period, for the biennial band (a), and the bidecadal band (b). Light gray describes positive values and dark gray is associated with negative values.

modes: a negative feedback that maintains the oscillatory nature, and a memory that determines the time-scale of the mode. When a positive feedback is also involved it increases the amplitude of the mode.

In a deterministic framework, as considered here, an internal oscillation within the climate system is therefore closely linked to a negative feedback. Following this idea, we refer to an internal mode as ‘fundamental’ if it includes at least one negative feedback and if the physical processes involved in the feedback (involving also its memory) are responsible for the specific time-scale associated with the mode. We use the term ‘derived’ for a mode that results from interactions of two other modes. Fundamental modes appear only on the left-hand side of relation (1), while the derived modes can appear on both sides of relation (1).

The derived modes rely completely on the negative feedbacks of the fundamental modes from which they emerge. They may also be amplified by positive feedbacks. Therefore, a mode’s large amplitude is not necessarily an indication that the mode is fundamental, because positive feedbacks determine the amplitude of both fundamental and derived modes. On the other hand, the fact that the derived modes rely on feedbacks of fundamental modes implies that their phase changing is triggered by the fundamental modes. Practically, this means that derived

modes are phase-locked with the modes from which they originate. Therefore, phase-locking may be an indication that a mode results from an interaction between two other modes.

Fundamental modes have high amplitudes in the regions where they are generated, whereas the derived modes can be detected with high amplitudes in the areas where their associated selecting and amplifying mechanisms are particularly strong.

3. Application to the biennial variability

Deser and Blackmon (1993) have identified a SST tripolar structure that dominates the climate variability in the North Atlantic area. The tripolar pattern is associated with a QD (12–14 yr) and a biennial (2 yr) time-scale, as also emphasized by other authors (Xie and Tanimoto, 1998; Tourre et al. 1999). There is significant observational evidence for the SST variability on 10–14 yr time-scales in various parts of the Atlantic Ocean to be part of a coherent pan-Atlantic decadal oscillation, characterized by zonal bands of SST and wind anomalies stacked in the meridional direction. However, the presence of biennial variability is surprising.

Surface biennial climate variability has been identified in the Indo-Pacific sector (Meehl, 1987) and Atlantic basin (Barnett,

1991; Deser and Blackmon, 1993; Mann and Park, 1994) and several mechanisms have been proposed to explain the 2-yr period variability (Meehl, 1987; Li et al. 2001). One of the main features of the tropospheric biennial signal is its tendency for phase-locking with the annual cycle (Lau and Shen, 1988). Barnett (1991) emphasizes the global character of the biennial signal and suggests that global interactions have to be considered in order to explain the variability for this mode.

We will show that the 2-yr period variability can be understood in terms of two fundamental modes: the annual cycle and a very stable QD mode originating in the Atlantic basin (Dima et al. 2001). Our methodology is based on the statistical analysis of instrumental data sets.

3.1. Fundamental modes

A POP analysis (Hasselmann, 1988; von Storch et al. 1988) was performed on the Comprehensive Ocean–Atmosphere Data Set (COADS) SST (da Silva et al. 1994) for the Atlantic sector (80° W–0°, 0°–65° N) in order to identify dominant oscillatory modes. POP is a multivariate method used to empirically infer the characteristics of the space–time variations of a complex system in a high-dimensional space. The method is used to identify and fit a linear low-order system to a few parameters.

The data, extending over the period 1945–1989, were detrended and normalized prior to the analysis, and only time-scales longer than 5 yr were considered. The analysis reveals a very

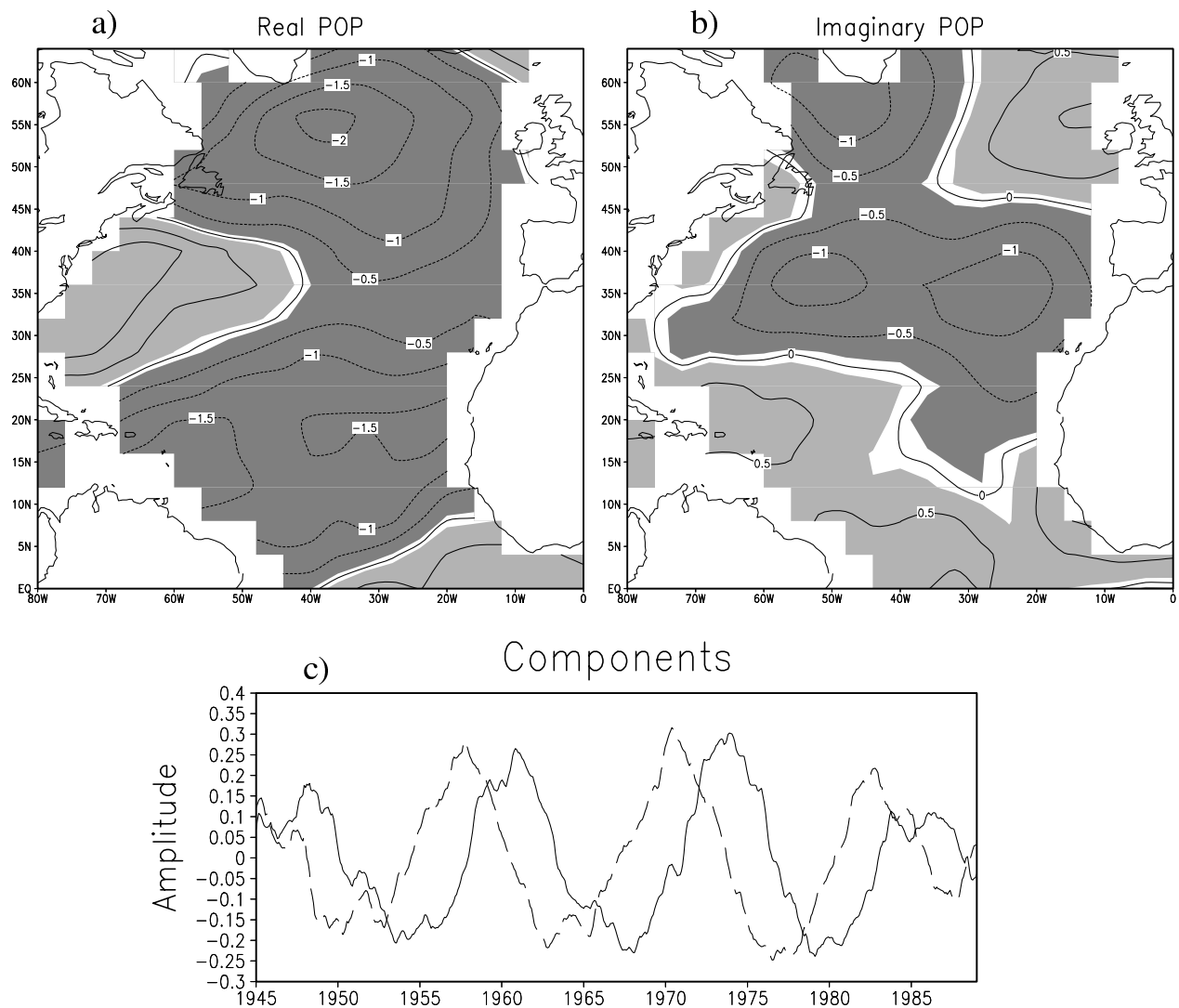


Fig 4. Real (a) and imaginary (b) parts of the dominant POP derived from the North Atlantic COADS SST data and their associated time components (c). The imaginary component is represented by a solid line and the imaginary component by a dashed line. The POP has a period of 13.1 yr and an e-folding time of 44.0 yr; it explains 21.6% of the variance. Prior to the analysis the data were detrended, normalized and a 5-yr running mean filter was applied.

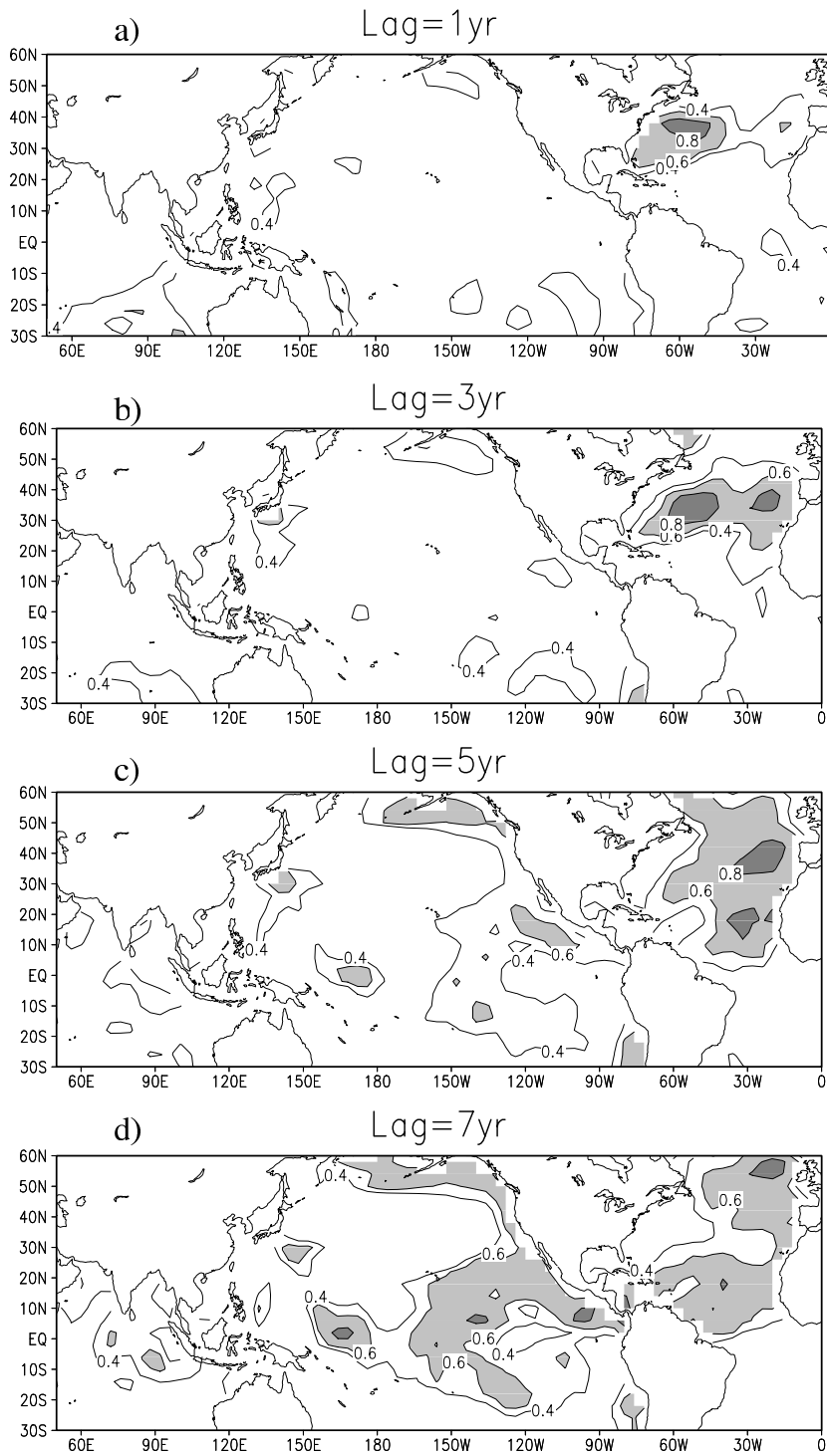


Fig 5. Lag correlation maps of the COADS SST field with a Gulf Stream SST Index (average over the 70°W – 60°W , 35°N – 40°N region); from top to bottom, the index leads the SST field by 1, 3, 5 and 7 yr. Prior to the correlation analysis, the data were detrended and a 5-yr running mean filter was applied. Correlations higher than 0.57 are statistically significant at the 95% level when nine degrees of freedom are considered.

stable mode with a period of 13.1 yr (Fig. 4). The POP's damping time is 44.0 yr, which indicates a very stable mode. The spatial structure (Fig. 4a) is very similar to that described by Deser and Blackmon (1993). The imaginary and real parts of the POP (Figs 4a and b) indicate the propagation of SST anomalies from the Gulf Stream region along the gyre circulation. Evidence

for the Gulf Stream SST anomalies to be transferred from mid-latitudes into the tropics through surface advection is further supported by a lag correlation analysis between a Gulf Stream SST Index and the COADS SST field (Fig. 5). The index was obtained as an average of the SST field over the 70°W – 60°W , 35°N – 40°N region, where the QD mode explains maximum variance, up to

90% (Dima et al. 2001). For the analysis, a 5-yr running mean filter was applied to the time series. Correlations higher than 0.57 are significant at the 95% level when nine degrees of freedom are considered. The correlation maps obtained (Fig. 5) show the propagation of the surface thermal anomalies in the Atlantic subtropical gyre; after propagating eastward, the signal evolves northward and southward where it meets the tropical region of the Atlantic. These tropical anomalies affect the tropical convection in the Atlantic sector (Czaja and Frankignoul, 2002; Terray and Cassou, 2002) and the atmospheric circulation at midlatitudes. This anomalous circulation provides for SST anomalies of reverse sign in the Gulf Stream region turning the cycle into its opposite phase (Fig. 4a, with reversed sign). Together with the POP analysis (Fig. 4), the lag correlation maps support the mechanism proposed to explain the Atlantic 13-yr mode as a coupled air–sea mode (Dima et al. 2001).

Figure 5 also shows that the SST anomalies become transferred into the Pacific and Indian basins when the signal reaches the tropical Atlantic realm. This is consistent with the idea that the Intertropical Convergence Zone (ITCZ) acts as a zonal waveguide through which the phase of the decadal signal is propagating westward (White and Cayan, 2000). Within a 7-yr time lag, the signal is dominant in the northern tropical Atlantic and tropical Pacific (Fig. 5). The signature of the Atlantic mode in the Pacific basin closely resembles the decadal Pacific mode described in several studies (Zhang et al. 1997). A regression of the time component associated with the QD mode derived from an EOF analysis on the Atlantic SST fields, onto the global SST, exhibits the same decadal pattern as in Fig. 5d (not shown).

Based on the observational evidence given by the POP analysis and the correlation maps, we consider the Atlantic QD cycle a fundamental mode, as is also the case for the annual cycle. Considering the 1-yr and 13.1-yr modes as fundamental, and using eqs (2a) and (2b), the periods obtained for the derived modes are 1.9 and 2.2 yr. The obtained derived periods are very close and both have biennial time-scales.

To obtain the atmospheric patterns associated with the fundamental modes (the annual cycle and the QD mode), we perform two EOF analysis on the North Atlantic (80°W–0, 0–70°N) COADS sea level pressure (SLP) fields covering the 1945–1989 period (da Silva et al. 1994). Prior to the computation, the linear trend was removed at each grid point and the data was band-pass filtered between 7 and 17 months for the annual cycle and between 9 and 15 yr for the QD mode. Note that the biennial time-scale has been excluded. The patterns and associated time series are displayed in Figs 6a–d. The first EOF for the 7–17 month band explains 60% of the total variance and exhibits a monopolar structure with maximum values south-east of Greenland (Fig. 6a). The time component is clearly dominated by annual variability. For the decadal band, the first EOF (60.0%) has a North Atlantic Oscillation (NAO) like dipolar structure (Hurrell, 1995) centered at 55°N (Fig. 6d); regressing the Atlantic SSTs onto the associated PC1 gives a pattern typical for the 13-yr

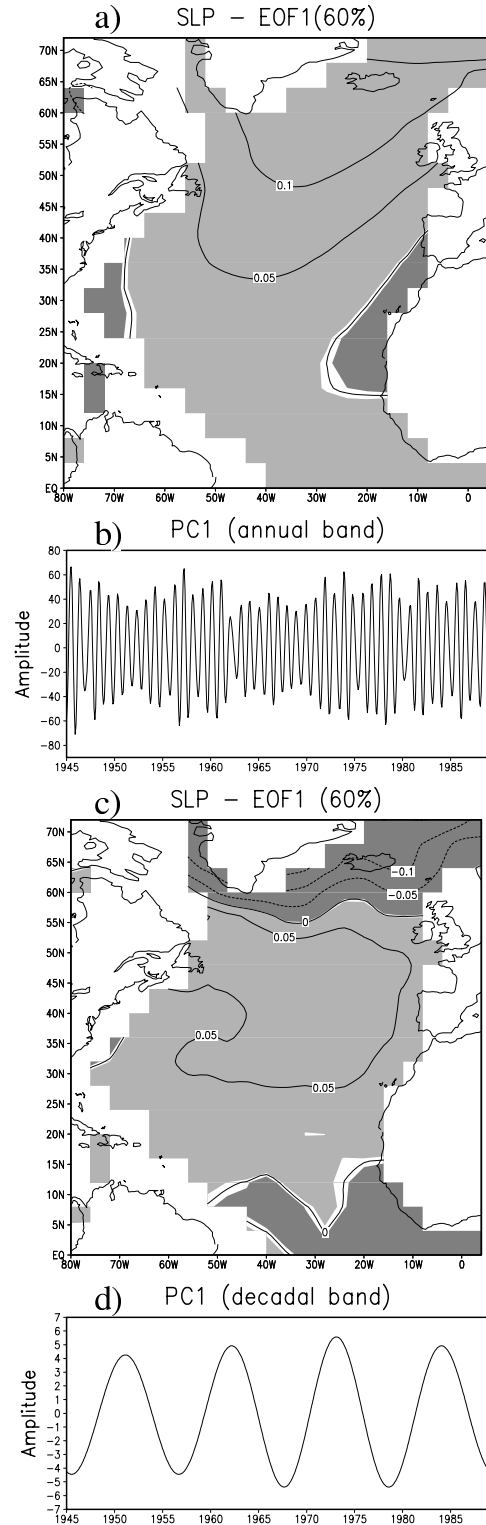


Fig 6. First EOF (a) and PC (b) of the North Atlantic COADS SLP field characteristic for the annual band; the first EOF (c) for the decadal band and the corresponding time component (d). Prior to the analysis the field was normalized by the temporal standard deviation at each grid point.

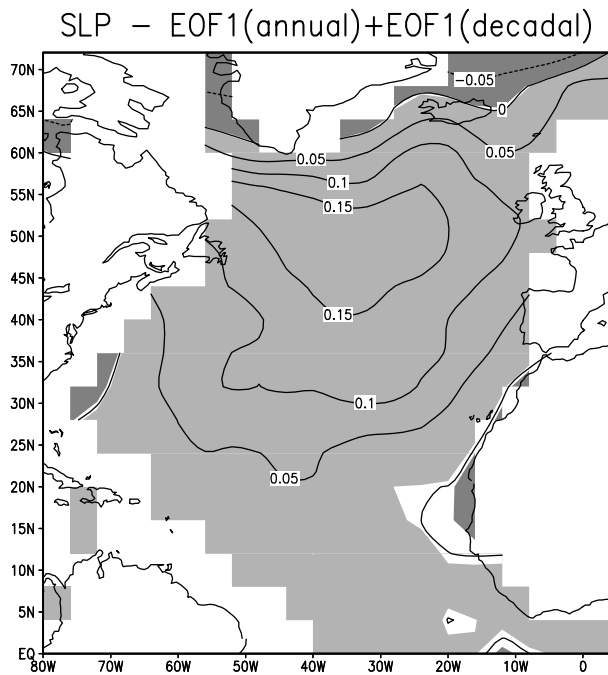


Fig 7. Sum of the first EOFs obtained from separate analysis on the SLP field, for annual (Fig. 6a) and decadal (Fig. 6c) bands.

mode, as shown by the real POP in Fig. 4a. The QD variability is evident in the PC1 time series (Fig. 6d). Our next step is to study the derived modes associated with the interaction between the annual cycle and the QD mode.

3.2. Derived modes

Considering the left-hand side of eq. (1), the spatial structure of the derived modes (Fig. 7) is obtained through a point-to-point addition of the patterns associated with the annual cycle (Fig. 6a) and the QD mode (Fig. 6c). The resulting structure (Fig. 7) shows a positive center shifted northward relative to that in Fig. 6a. This pattern is projected onto the unfiltered COADS SLP field in order to derive its associated time component. Prior to the projection, monthly anomalies relative to the climatological values were calculated, therefore removing the seasonal cycle. The projection of the superposition pattern onto the SLP data shows pronounced interannual variability (Fig. 8a). A SSA (Allen and Smith, 1997) was performed to determine the dominant components in the projection time series. The SSA method is used to determine a set of empirical basis functions in the time domain which can be shown to converge to the standard Fourier functions (sine and cosine) as the time series increases in length. The advantage of using the SSA obtained functions over using sine and cosine is that these functions are not necessarily harmonic but data adaptive, and thus they can capture highly anharmonic oscillation shapes (Ghil et al. 2002). The technique may be visualized by sliding a window of chosen width (M) down a time

series while determining the orthogonal patterns that best capture the variance in the time component. The SSA method is generally used to identify trends, oscillatory patterns and noise in time series (Allen and Smith, 1997) and will be extensively used in the present study. As a rule of thumb, the length of the window, M , should be chosen to be longer than the number of points in the oscillatory periods under investigation and shorter than the number of data points in the spells of an intermittent oscillation (Vautard et al. 1992). Robustness of results to variation of M is an important test for their validity (Dettinger et al. 1995). Repeated SSA analysis show that quasi-periodic signals are efficiently identified using windows several times longer than their periods. In all our further SSA analyses, the identified quasi-periodic components are insensitive to reasonable variations of window length. In the present analysis we use an 80-month window.

The eigenvalue spectrum (Fig. 8b) indicates that the first two dominant components describe a standing oscillation, because the eigenvalues are very close to each other (Vautard et al. 1992). This is confirmed by the time-EOFs (Fig. 8c) associated with the first two eigenvalues, which are phase-shifted by 90° , typical for a standing oscillation. The reconstructed time series based on the first two SSA components (Fig. 8d) is dominated by biennial variability. Its maximum entropy method (MEM; Burg, 1978; Childers, 1978) spectrum shows a 2.5-yr period (not shown), in good agreement with the periods of the derived modes and with the typical time-scale of the biennial variability.

In order to obtain the spatial fingerprint of the biennial mode, we calculate composite maps based on the (detrended, normalized and biennial-band filtered) SST and SLP fields and on the reconstructed biennial component (Fig. 8d). Because the obtained biennial variability is, by construction, based on modes identified in the Atlantic basin, the maximum amplitudes in the SLP regression map (Fig. 9b) are detected in the North Atlantic region. In the tropical Pacific, the signature of the Southern Oscillation (Philander, 1990) is detected in the SLP field (Fig. 9b), and an ENSO-like pattern is observed in the SST regression map (Fig. 9a). Very similar maps are obtained as leading modes (not shown) in two EOF analyses performed in the biennial band on the SST and SLP fields. A similar procedure performed using the SLP fields from Trenberth and Paolino (1980) for the 1945–1999 period provides qualitatively the same results (not shown), suggesting that our analysis is not sensitive to the data used.

4. Application to interannual variability

4.1. Second-order derived modes

Next we consider the interactions between the QD mode, considered a fundamental mode, and the biennial cycle, a first-order derived mode. In Section 3, in which the biennial variability is derived, results based on COADS SST fields are presented. They cover a post World War II period (1945–1989),

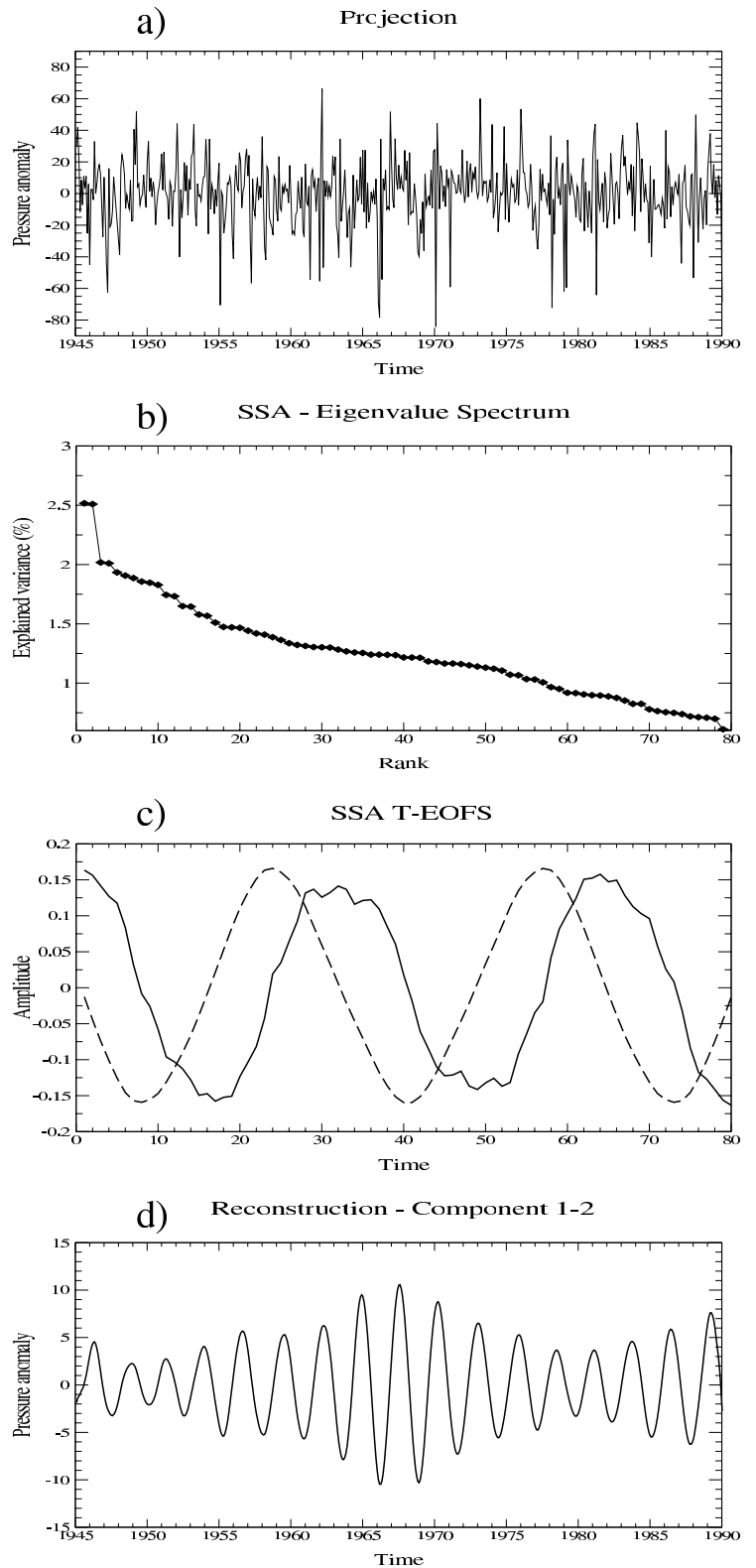


Fig 8. Analysis of the time component associated with the pattern in Fig. 7. (a) Projection of the map in Fig. 7 onto the unfiltered COADS SLP field. (b) Eigenvale spectrum obtained from a SSA, using an 80-month window. (c) First pair of time-EOFs; the unit on the time axis is 1 yr. (d) Reconstructed component associated with the first pair of time-EOFs.

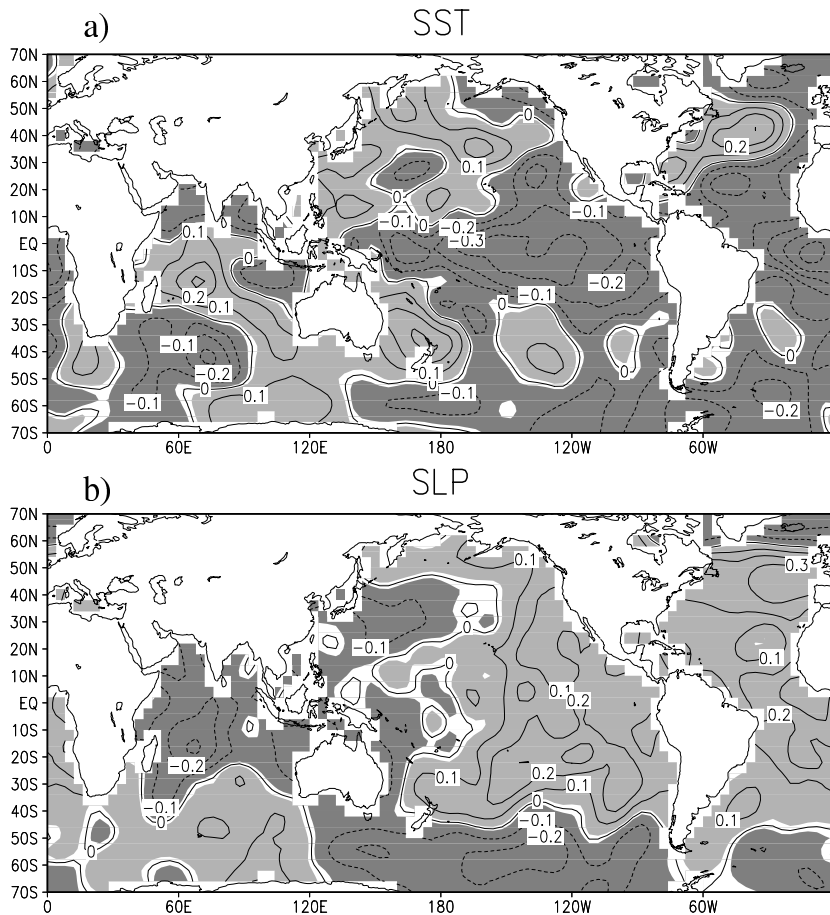


Fig 9. Composite maps constructed based on the reconstructed component in Fig. 8d and the COADS SST (a) and SLP (b) fields; both fields were detrended, normalized and filtered in the biennial band.

assuring a maximum possible data quality. However, when analyzing derived modes with longer characteristic time-scales, longer data sets are necessary. Therefore, in order to test the generation of second-order derived modes, monthly SST and SLP fields of Kaplan et al. (1998) for the 1856–1991 period are used. Prior to the analysis, the linear trend is removed, fields are normalized by their temporal standard deviations at each grid point and data are filtered so that only time-scales between 7–31 months and 9–14 yr are retained, respectively.

In order to identify the dominant global coupled SST–SLP patterns associated with the biennial (7–31 months) and the QD modes, coupled simultaneous ocean–atmosphere patterns over both basins are identified in the two fields using two CCAs (von Storch and Zwiers, 1999) performed in the 7–31 month and 9–14 yr bands, respectively. Note that the 4- and 6-yr time-scales are excluded from the analysis. The CCA method is used here to identify dominant coupled ocean–atmosphere patterns because for the modes under consideration, having interannual time-scales, the air–sea interactions are essential.

The dominant SST (23.8%) and SLP (34.8%) coupled patterns corresponding to the 7–31 month bands are presented in Fig. 10. The SST field (Fig. 10a) has an ENSO-like structure with negative anomalies extending westward from the South Ameri-

can coast to the 160°E longitude and with positive values over the central North Pacific. In the Atlantic sector, a band of negative anomalies extends between the equator and 30°N. The SLP field (Fig. 10b) resembles the Southern Oscillation structure in the Pacific while negative anomalies are observed in the tropical Atlantic. The associated SST and SLP time series (Fig. 10c) are highly correlated (0.89) and show pronounced interannual variability.

For the 9–14 yr band, the dominant SST pattern (Fig. 11a) explaining 33.7% of the variance in the Atlantic sector (30°S to 60°N) is characterized by zonal bands with alternating sign (Fig. 11a). Such a pattern is typical for the Atlantic 12–14 yr cycle (Deser and Blackmon, 1993; Dima et al. 2001). The SLP pattern (37.0%) is also consistent with this cycle, with a western Atlantic Oscillation like structure. The SST field has maximum values in the center of the Pacific sector (between 170°E–130°W, 10°S–10°N) while pronounced negative anomalies occur in the central North Pacific. The SST and SLP time series (Fig. 11c) are highly correlated (0.94) and they show enhanced QD variability. The features of this coupled pattern, like its 12–14 yr characteristic time-scale and SST and SLP patterns in the Atlantic sector, argue for associating these coupled patterns with the Atlantic QD mode.

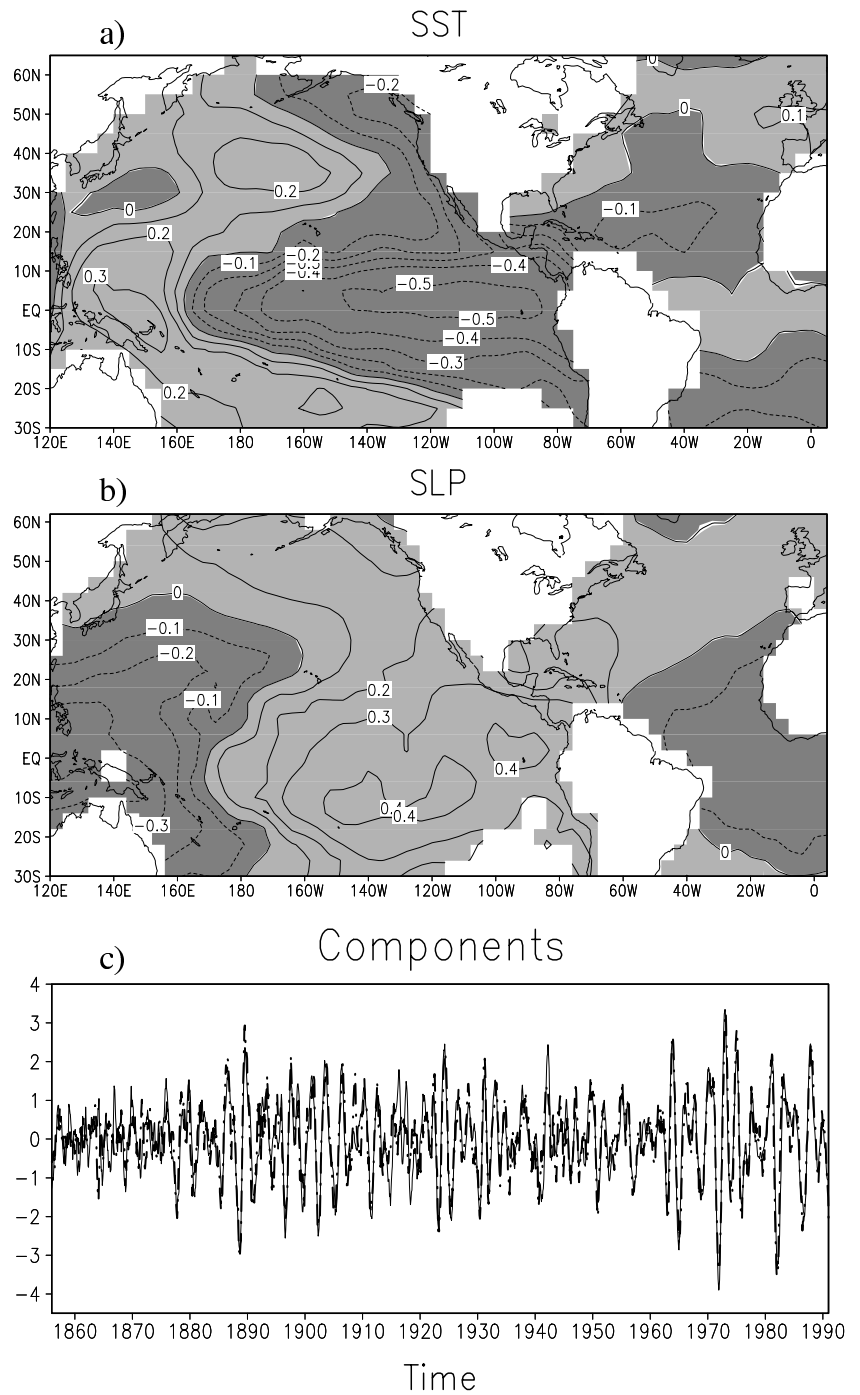


Fig 10. Dominant coupled modes obtained through CCA of the SST and SLP fields from Kaplan et al. (1998). The analysis is performed in the biennial band. Prior to the analysis the fields were normalized by the temporal standard deviation at each grid point. (a) SST map; (b) SLP map; (c) associated time components, SST (solid) and SLP (dots).

In order to derive the specific structure associated with the superposition between the main modes of variability in the Pacific and Atlantic basins, we linearly combine (addition) the two dominant SST patterns corresponding to the 7–31 month and 9–14 yr bands. The resulting SST field (Fig. 12a) presents features from both dominant SST patterns derived through the CCAs. In order to obtain the temporal variability corresponding to this pattern, and therefore the temporal variability associated with the combi-

nation between the two modes, we project the initial (unfiltered) SST field onto this map. Prior to the projection, the SST field was detrended and normalized by the standard deviation at each grid point. The projection of the ‘interaction’ pattern onto the SST field is shown in Fig. 12b. The signal is characterized by high interannual variability.

Furthermore, an SSA is performed on this time series using a 30-yr window, in order to identify the dominant oscillatory

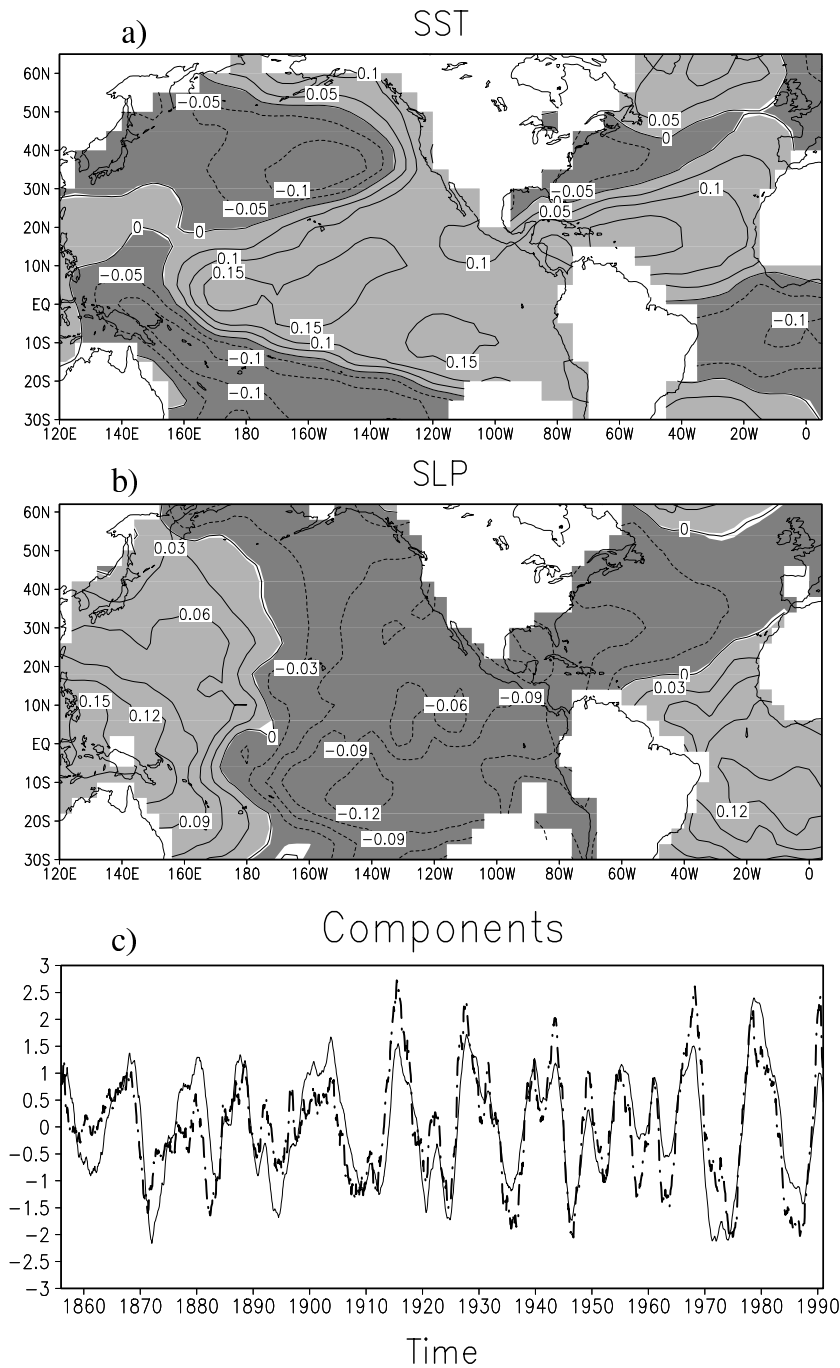


Fig 11. As in Fig. 10, but the analysis is performed for the decadal band.

signals embedded within. The eigenvalue spectrum (Fig. 13a) emphasizes two pairs of dominant values. The time-EOFs associated with the first and second eigenvalues (Figs 13b and c) describe a standing oscillation with a 6.2-yr period, identified using the MEM analysis. The second dominant oscillatory component (the second pair of eigenvalues; Figs 13d and e) also describes a standing oscillation with a 3.6-yr period. These periods are very close to the 4.2- and 6.2-yr modes obtained using eq. (2) with $T_1 = 2.5$ and $T_2 = 13.1$ yr.

Our results are also supported by observational evidence (Rogers, 1984; Huang et al. 1998) that the tropical Pacific indices (SOI and Niño3) and the NAO index show significant coherence in the 2–4 and 5–6 yr frequency bands. The SST and SLP patterns associated with these second-order derived modes are obtained by constructing composite maps based on the Kaplan et al. (1998) SST and SLP fields and the SSA reconstructed time components. The fields are detrended and filtered in the ~ 3 –5 band (for the 4-yr mode) and in the ~ 5 –7 yr band

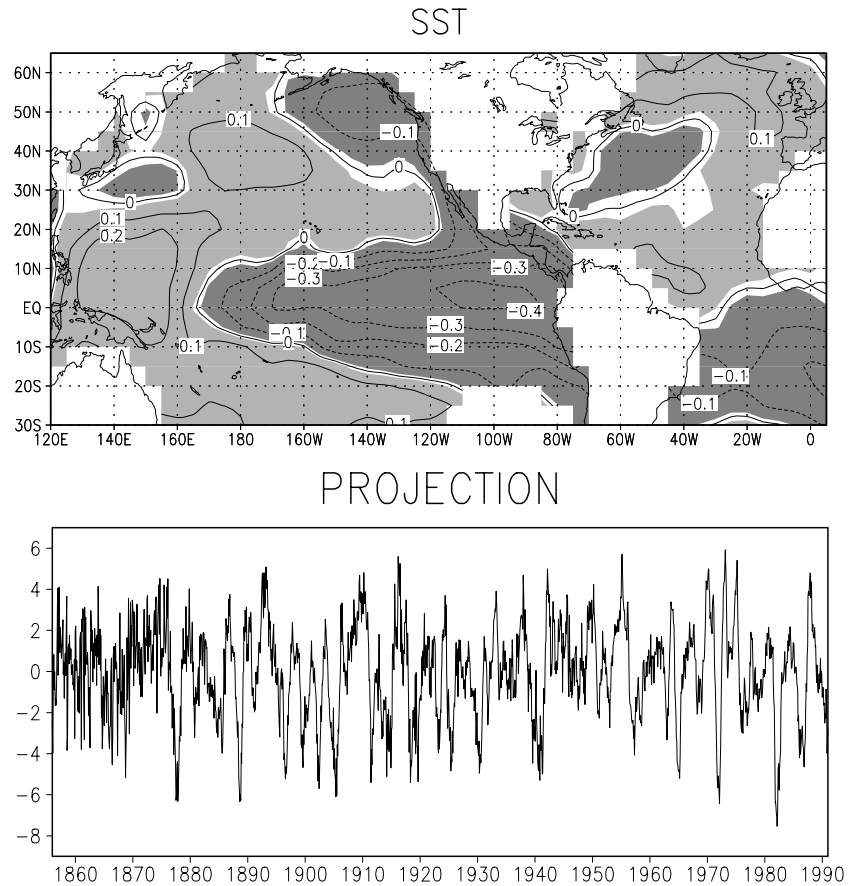


Fig 12. (a) Sum of the first SST patterns obtained from the two CCAs, corresponding to biennial and to decadal bands, displayed in Figs 10a and 11a, respectively. (b) Projection of the map in Fig. 12a onto the unfiltered SST field.

(for the 6-yr mode). The SST pattern corresponding to the 4-yr mode (Fig. 14a) has an ENSO-like structure in the Pacific basin while a tripole-like structure is detected in the Atlantic sector. Note that this 4-yr time-scale is also discernible in the spectrum presented by Deser and Blackmon (1993) in association with the tripole structure. The corresponding SLP structure (Fig. 14b) has a Southern Oscillation like pattern in the Pacific Ocean and a Western Atlantic structure in the Atlantic basin. The patterns associated with the ~6-yr mode are similar to the 4-yr maps in the Pacific region. We have applied different techniques (EOF and CCA) to derive the biennial, 4- and 6-yr modes and find that our results are not sensitive to the statistical methods used in analyses.

4.2. Third-order derived modes

The large amplitudes of the 4- and 6-yr modes (as second-order derived modes) in the tropical Pacific suggest that third-order modes may also be generated in a similar manner. To test this hypothesis we combine (addition) the SST fields associated with the 13-yr fundamental mode (obtained through CCA) and the 6-yr mode. This latter mode was obtained from a CCA analysis on the SST and the SLP fields, filtered to retain time-scales in the 5–7 yr band (not shown). Similar results are obtained if a

composite SST map, based on the 6-yr component derived from SSA (Fig. 13c), is used. The resulting map (Fig. 15a) is then projected onto the detrended and normalized annual mean SST field to obtain the associated time component (Fig. 15b). This time series was smoothed using a 3-yr running mean filter and then a SSA analysis was performed on it, using a 40-yr window. The time-EOFs and the reconstruction of the first and the third dominant components are presented in Fig. 16. The second component (not shown) is associated with the 13-yr mode. The first and third components appear as standing oscillations (Figs 16a, b, c and d, respectively) and are characterized by periods of approximately 20 and 9 yr, respectively. When combining the 6.2- and 13.1-yr modes, the fundamental and derived mode concept gives third-order modes of 23.5- and 8.4-yr periods, very close to the values obtained above (20 and 9 yr). The SST and SLP composite maps associated with these components are shown in Fig. 17. They were obtained based on the reconstructed time components and annual SST and SLP fields from Kaplan et al. (1998). The fields were detrended and a 3-yr running mean filter was applied to remove the relatively high-frequency variability. The SST map associated with the 8-yr mode (Fig. 17a) has a tripole structure in the North Atlantic and a center of negative anomalies in the North Pacific close to the western part of the North American coast. The SLP field (Fig. 17b) has a NAO-like (Hurrell, 1995)

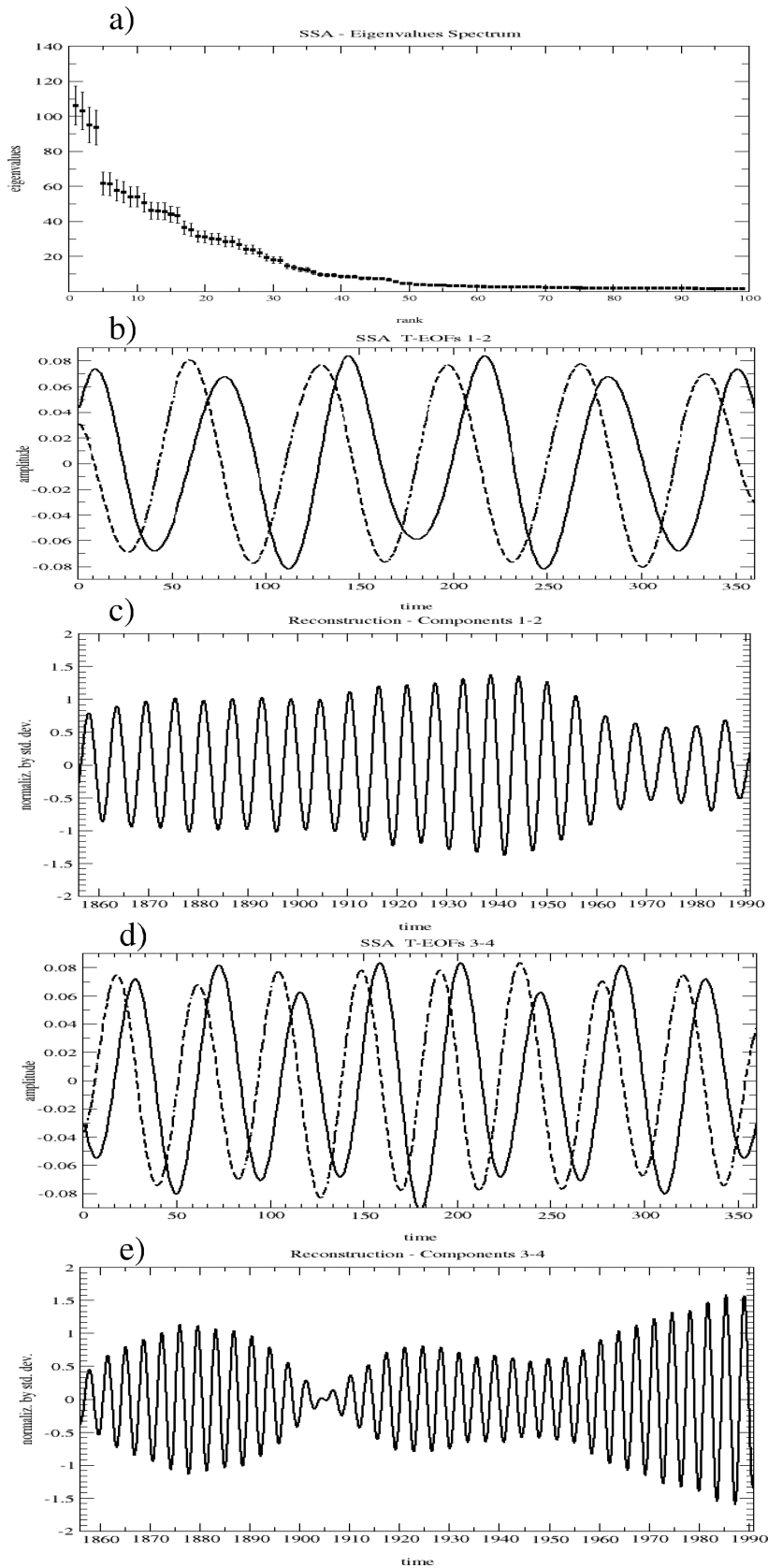


Fig 13. SSA of the time series in Fig. 12b. (a) Eigenvalue spectrum obtained from a SSA analysis using an 80-month window. (b) First pair of time-EOFs; the unit on the time axis is 1 yr. (c) Reconstructed component associated with the first pair of time-EOFs. (d) Second pair of time-EOFs; the unit on the time axis is 1 yr. (e) Reconstructed component associated with the second pair of time-EOFs.

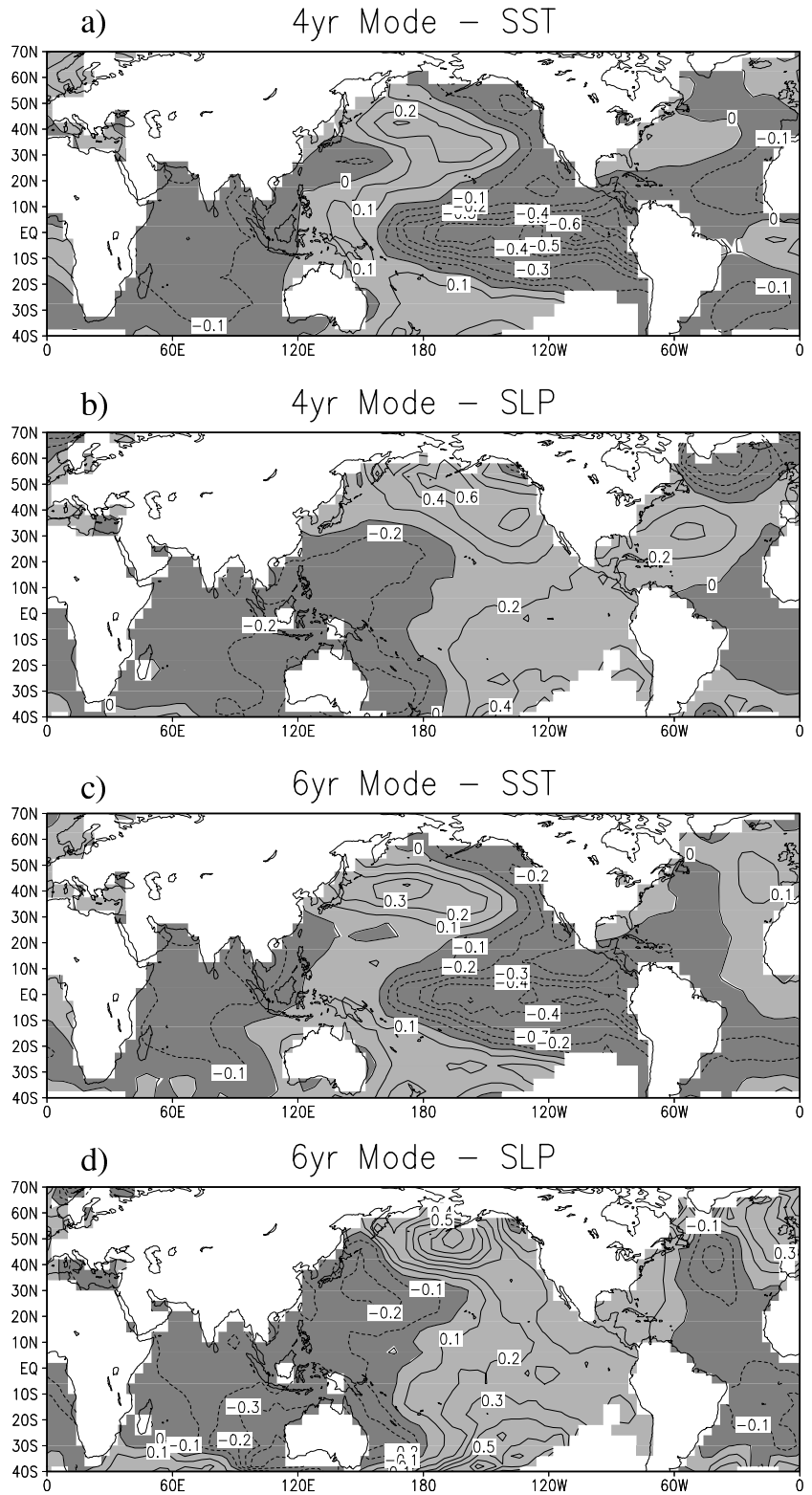


Fig 14. Composite maps of the reconstructed component in Fig. 13e based on the Kaplan SST (a) and SLP (b); composite maps of the reconstructed component in Fig. 13c based on the Kaplan et al. (1998) SST (c) and SLP (d). The SST anomalies are expressed in degrees and the SLP anomalies in hPa.

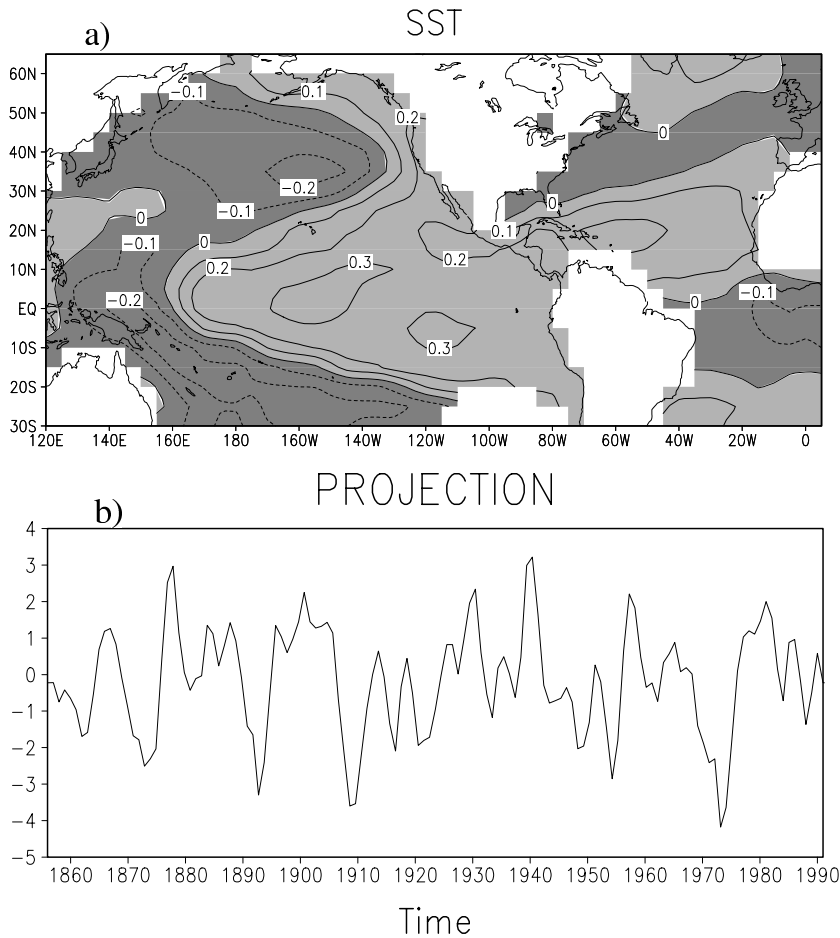


Fig 15. (a) Sum of the first SST patterns obtained from two CCAs, corresponding to the 5–7 and 9–14 yr bands. (b) Projection of the map in Fig. 15a on the detrended and normalized annual mean SST field.

structure, consistent with studies showing this particular time-scale to be observed within the NAO variability (Rogers, 1984). The SST ENSO-like pattern (Zhang et al. 1997) is observed in the map associated with the bidecadal mode (Fig. 17c). Note that bidecadal variability was reported in the Atlantic sector by Cook et al. (1998).

Therefore, the concept of fundamental and derived modes is in good agreement with the observational results when considering higher-order (second and third) derived modes. It is worth noting that, as the time-scale of the modes increases from a 2-yr to a 23-yr period (Figs 3, 14 and 17), the meridional extension of the SST anomalies centered in the eastern tropical Pacific extends further and further. The waveguides of Rossby waves may be responsible for this meridional extension and support the ‘selection’ mechanism as part of our concept.

Also consistent with the waveguide notion, as the time-scale increases, the maximum amplitude of the SST anomalies moves from the tropical Pacific (in the case of the 2- and 4-yr modes) to the North Pacific (in the case of the 6-, 8-, and 23-yr modes). The large SST anomalies in these two regions may also be favored by local positive feedbacks that optimally amplify these specific time-scales. Such feedbacks were identified by Philander (1990)

in the tropical Pacific and by Seager et al. (2001) in the North Pacific Ocean.

Interestingly, as the period of a derived mode is closer to that of the fundamental mode from which it originates, its associated patterns are more similar to that of the fundamental mode. For example, the SST map associated with the 8-yr mode (Fig. 17) shares, in the Atlantic basin, more common features with the pattern of the 13-yr mode (Fig. 11) than the 4- and 6-yr modes (Fig. 14) share with the QD mode. This brings additional support to our concept.

5. Conceptual features of the mode interactions

In the framework of our concept, it is worth evaluating the factors that may contribute to the amplitude of a mode at a given location. For this purpose we propose an analogy involving two wave sources placed in distinct points (Fig. 1). These sources are virtually associated with two fundamental climate modes. One may assume that each of the sources generates a wave field, in a similar way as the fundamental modes generate quasi-periodic climate signals. These signals may be damped or amplified as they propagate. A typical climate problem would be to identify

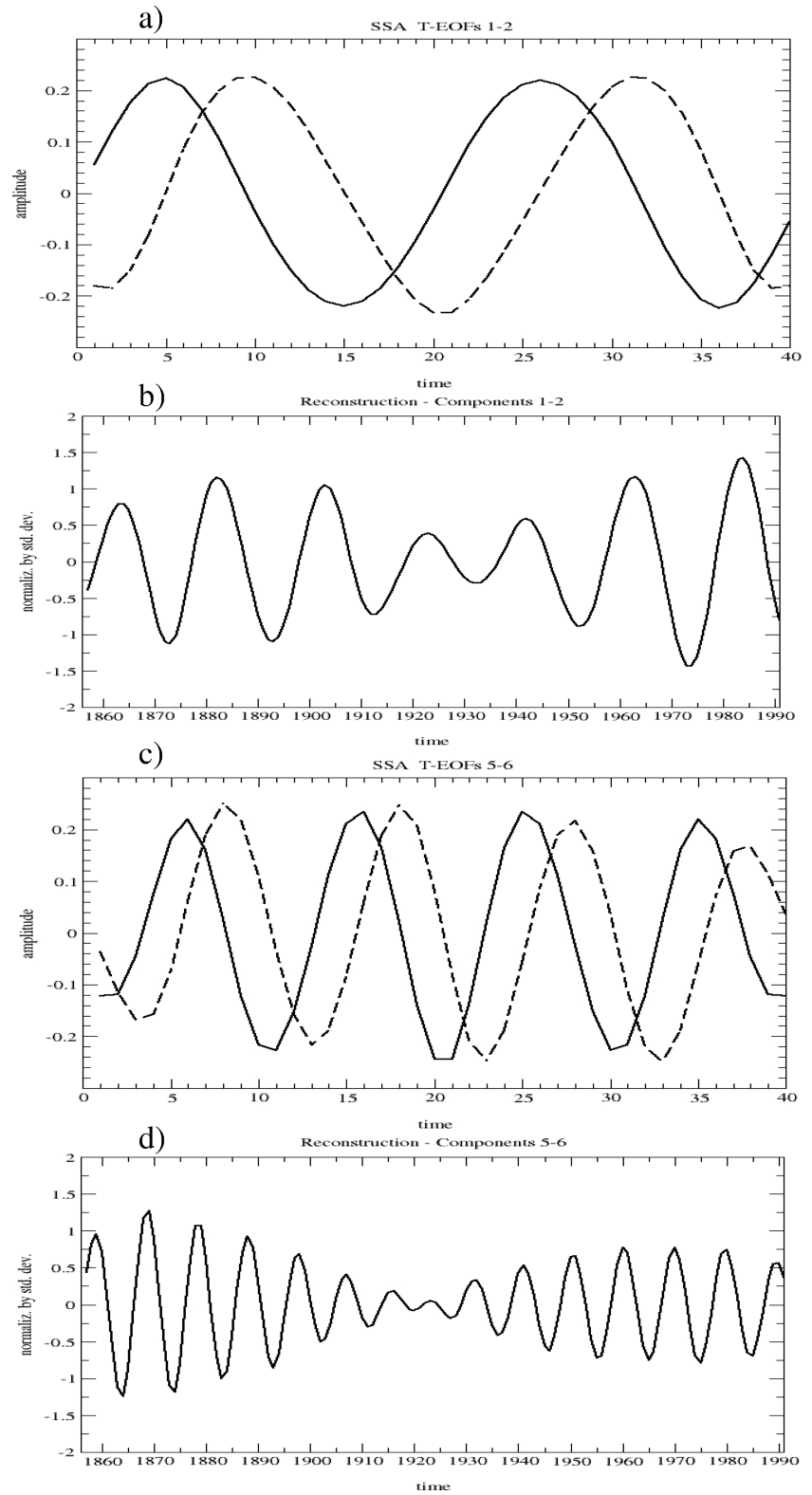


Fig 16. SSA of the time series in Fig. 15b. (a) First pair of time-EOFs. (b) Reconstructed component associated with the first pair of time-EOFs. (c) Third pair of time-EOFs. (d) Reconstructed component associated with the third pair of time-EOFs.

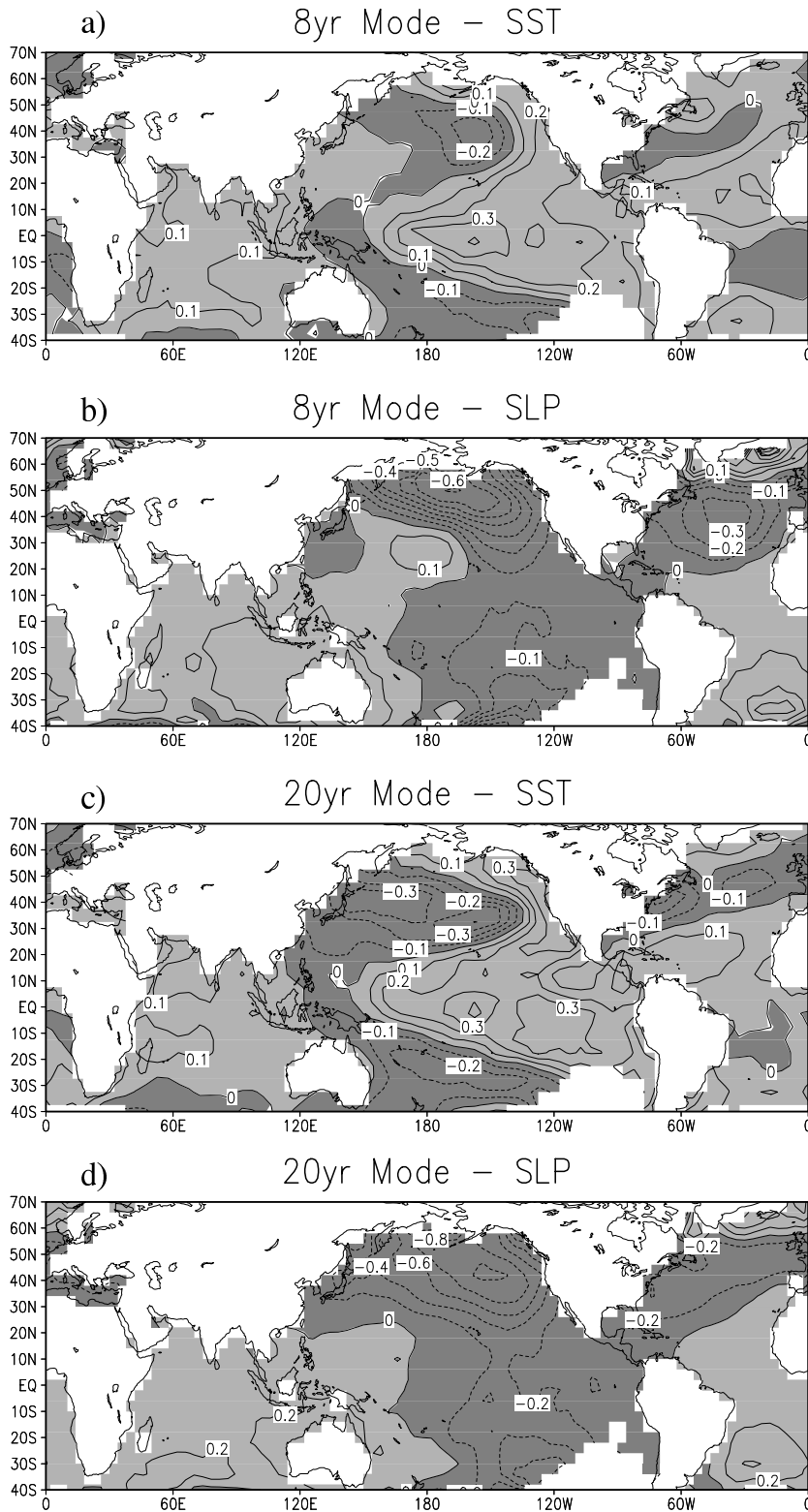


Fig 17. Composite maps of the reconstructed component in Fig. 16d based on the Kaplan et al. (1998) SST (a) and SLP (b); composite maps of the reconstructed component in Fig. 16b based on the Kaplan et al. (1998) SST (c) and SLP (d). The fields were normalized by the standard deviation at each grid point.

the signal produced by each source by analyzing the field that results from the combination between the fields generated by each mode. The best location for detecting the first source is point 1. Similarly, the best location for detecting the second source is point 2. At locations far enough from both sources, the dominant signal would be associated with the superposition between the two sources (e.g. points A and B). By analogy, the signals associated with fundamental modes are easily identified in regions where the modes originate, while in other regions the resulting derived modes dominate. As a possible application, a multivariate EOF analysis would emphasize the fundamental modes if the analysis is performed over regions where these modes originate. However, if the same analysis is performed over regions where no fundamental modes originate, or over regions that include the 'sources' of two or more fundamental modes, then it would most likely emphasize the derived modes. Therefore, the first two factors that influence the detection of the modes are the 'position' and the 'extent' of the analyzed region with respect to the location of the sources for the fundamental modes.

In our study, all the modes considered are in connection to the annual and QD cycles, as fundamental modes. The connections were put into evidence through multiple iterations of our concept: three combinations of modes result in periods in the 4- and 6-yr bands, while two combinations are associated with the 8- and 23-yr modes, respectively. This is consistent with observational evidence which shows that the tropical Pacific variability (as, for example, described by the Niño3 index) is dominated by time-scales of 4 and 6 yr. Also, the 8- and 23-yr time-scales are identified in both the Pacific and the Atlantic basin (Rogers, 1984; Cook et al. 1998). Therefore, a third factor that may influence the mode detection is the 'frequency overlapping' between two or more modes.

Another element to be considered is the possible positive feedbacks involved. For example, the coupled ocean-atmosphere tropical Pacific system may amplify even weak signals through ocean-atmosphere interactions (Bjerknes, 1969). A characteristic time-scale for such a positive feedback may be provided by particular physical processes such as oceanic adjustment to variable wind conditions, through Rossby and Kelvin wave propagation in the equatorial waveguide (Gill, 1982). If we consider that these derived modes are efficiently amplified by the positive feedback generated by ocean-atmosphere interactions in this sector, then the dominance of the 4- and 6-yr time-scales in the tropical Pacific is a natural consequence. Therefore, the fourth element that may influence mode detection is related to 'local feedbacks' that may amplify the signals. These local feedbacks may also be viewed as resonances between global modes and location-specific growing modes.

A standard inference from statistical analyses of climatic data is that a mode originates in a particular region if it explains a large percentage of the variance in that area. However, in our view, if the mode considered is a derived one, then large percentages of explained variance are not necessarily an indication for the

origins of the mode in that specific region. Most likely, the correct inference would be that the derived mode is efficiently amplified by local positive feedbacks in that region. Moreover, it is natural to expect that in the region where a fundamental mode has its origins, the potential derived modes do not explain an important part of the variance.

The above considerations may be part of a picture in which the ENSO phenomenon appears as an amplification and overlapping of derived modes in the tropical Pacific coupled ocean-atmosphere system. Such a picture is in agreement with the concept that ENSO results from interactions between multiple time-scales in the tropical Pacific (Barnett, 1991). However, an important consequence resulting from applying the fundamental and derived mode concept to the tropical Pacific is that the negative feedback (necessary in changing the phase of the mode) does not necessarily originate in the tropical Pacific sector. Overall, the picture constructed based on our concept is in agreement with previous observational studies that have successfully described the positive feedback in the tropical Pacific (Bjerknes, 1969), while no conclusive observational evidence was yet presented for a potential negative feedback in this region (Fedorov and Philander, 2001).

6. Conclusions

In the present study we propose a concept of mode interactions. The concept is based on the distinction between fundamental and derived modes of climate variability and assumes that the 'fundamental' modes can be combined in the Fourier space in order to obtain 'derived' modes of variability. As a first application, we considered the annual cycle and the QD mode to be fundamental. Using SLP fields we showed that the biennial variability results from an interaction between the two fundamental modes, which is in agreement with the periods provided by our theory. Similar results are obtained when analyzing different data sets.

Specific spatial features associated with the biennial climate variability are well explained by our concept. For example, the surface biennial variability has a clear signature in the tropical belt, but does not have a global signature in the midlatitude SLP field. The only midlatitudinal region where the biennial variability has a significant fingerprint is the North Atlantic region (Barnett, 1991); here the mode shows a very coherent structure, which is easy to understand considering that the mode originates from the interaction between the annual cycle and the North Atlantic QD mode. In accordance with our concept, the strong biennial signal reported in the Indian Ocean goes together with the large amplitudes of the annual cycle in that region. The phase-locking between the annual cycle and the biennial variability (Lau and Shen, 1988) is also consistent with our interaction model. The decadal modulation of the global biennial mode appears as a natural consequence in our concept (White and Allan, 2001).

We further applied the fundamental and derived mode concept to the interannual variability. Based on the biennial and on the

QD modes, it is shown that second-order derived modes (with periods of about 4 and 6 yr) and third-order derived modes (with periods of about 8 and 23 yr) are thus being generated.

To summarize, we can construct a scheme for the application of our fundamental and derived mode concept:

(1 yr, ~13 yr) => (~2 yr, ~2 yr)
 (~2 yr, ~13 yr) => (~4 yr, ~6 yr)
 (~6 yr, ~13 yr) => (~8 yr, ~23 yr).

We suggest that the large amplitude and/or the large percentage of the variance explained by a mode in a region is not necessarily an indication for the mode originating in that region. This inference may be valid for a fundamental mode, if the analysis is performed in the region where it originates, but it is not necessarily valid for a derived mode. The fundamental and derived mode concept emphasizes two elements that may explain the prominence of the 4- and 6-yr modes (as second-order derived modes) in the Pacific basin: the overlapping of the frequencies of several derived modes and a local positive feedback which optimally amplifies the modes characterized by these time-scales.

In our view, the derived modes depend essentially on the physics of the fundamental modes. Therefore, the negative feedbacks changing the phase of a derived mode are locked to the fundamental modes. Then, an important consequence of the application of the fundamental and derived mode concept to inter-annual variability is that the negative feedback responsible for the generation of interannual variability in the tropical Pacific does not necessarily originate in the Pacific basin. Note that the phase-locking of the ENSO mode to the annual cycle appears as a natural consequence of our concept. Moreover, phase-locking provides support for a deterministic origin of the considered modes. In this view, the Pacific basin appears as a ‘resonator’ that optimally amplifies modes with specific time-scales (e.g. interannual variability).

Our concept emphasizes that the variability of the derived modes stems from that of the fundamental modes and from the inherent climate resonances at certain time-scales. These resonances are connected to internal dynamics, as for example the wave dynamics in the tropical Pacific. As in the framework of the stochastic climate model (Hasselmann, 1976), our deterministic perspective on climate variability is based on the interaction of the climate components with different typical time-scales. While in the stochastic paradigm an important problem is identifying the stabilizing feedback limiting the amplitude of the climate signals, in the framework of our concept the main points are related to the identification of the fundamental modes and of the selection mechanisms. Therefore, we believe that our deterministic concept complements the stochastic paradigm. As a natural further step, future studies will concentrate on the application of our concept to longer time-scales and on the implications of the results on climate predictability.

7. Acknowledgments

We wish to thank to Dr Norel Rimbu for useful discussions, and two anonymous reviewers for their constructive suggestions. This research was funded by the Bundesbildungsministerium für Bildung und Forschung through DEKLIM and by the Deutsche Forschungsgemeinschaft as part of the Research Center ‘Ocean margins’ of the University of Bremen (No. RCOM0097).

References

- Allen, M. and Smith, L. A. 1997. Optimal filtering in Singular Spectrum Analysis. *Phys. Lett.* **234**, 419–428.
- Barnett, T. P. 1991. The interaction of multiple time scales in the tropical climate system. *J. Climate* **4**, 269–285.
- Bjerknes, J. 1964. Atlantic air–sea interaction. *Adv. Geophys.* **10**, 1–82.
- Bjerknes, J. 1969. Atmospheric teleconnections from the equatorial Pacific. *Mon. Wea. Rev.* **97**, 163–172.
- Burg, J. P. 1978. Maximum entropy spectral analysis. *Modern Spectrum Analysis*. IEEE Press, Piscataway, NJ, 42–48.
- Childers, D. G. 1978. *Modern Spectrum Analysis*. IEEE Press, Piscataway, NJ, 331 pp.
- Clement, A. C., Seager, R. and Cane, M. A. 1999. Orbital controls on ENSO and the tropical climate. *Paleoceanography* **14**, 441–456.
- Cook, E. R., D’Arrigo, R. D. and Briffa, K. R. 1998. A reconstruction of the North Atlantic Oscillation using tree-ring chronologies from North America and Europe. *The Holocene* **8**, 9–17.
- Czaja, A. and Frankignoul, C. 2002. Observed impact of Atlantic SST Anomalies on the North Atlantic Oscillation. *J. Climate* **15**, 606–623.
- da Silva, A., Young, A. C. and Levitus, S. 1994. *Atlas of Surface Marine Data 1994. Algorithms and Procedures*, Vol. 1. NOAA Atlas NESDIS 6, Washington, DC.
- Deser, C. and Blackmon, M. L. 1993. Surface climate variations over North Atlantic Ocean during winter: 1900–1989. *J. Climate* **6**, 1743–1753.
- Dettinger, M. D., Ghil, M., Strong, C. M., Weibel, W. and Yiou, P. 1995. Software expedients singular-spectrum analysis of noisy time series. *Eos. Trans. Am. Geophys. Union* **76**, 14–21.
- Dima, M., Rimbu, N., Stefan, S. and Dima, I. 2001. Quasi-decadal variability in the Atlantic Basin involving tropics-midlatitudes and ocean–atmosphere interactions. *J. Climate* **14**, 823–832.
- Einstein, A. 1905. Über die von der molekularkinetischen Theorie der Wärme geforderte Bewegung von in ruhenden Flüssigkeiten suspendierten Teilchen. *Ann. Phys.* **17**, 549–560.
- Fedorov, A. V. and Philander, S. G. 2001. A stability analysis of tropical ocean–atmosphere interactions: bridging measurements and theory for El Niño. *J. Climate* **14**, 3086–3101.
- Ghil, M. and Robertson, A. W. 2002. ‘Waves’ vs. ‘particles’ in the atmosphere’s phase space: A pathway to long-range forecasting? *Proc. Natl. Acad. Sci.* **99** (Suppl. 1), 2493–2500.
- Ghil, M., Allen, M. R., Dettinger, M. D., Ide, K., Kondrashov, D., et al. 2002. Advanced spectral methods for climatic time series. *Rev. Geophys.* **10**, 1029/2000GR000092.
- Gill, A. E. 1982. *Atmosphere–Ocean Dynamics*. Academic Press, New York, 662 pp.
- Hasselmann, K. 1976. Stochastic climate models. *Tellus* **28**, 473–484.

- Hasselmann, K. 1988. PIPs and POPs: The reduction of complex dynamical systems using principal interaction and oscillation patterns. *J. Geophys. Res.* **93**, 11 015–11 021.
- Huang, J., Higuchi, K. and Shabbar, A. 1998. The relationship between the North Atlantic Oscillation and El Niño-Southern Oscillation. *Geophys. Res. Lett.* **25**, 2707–2710.
- Hurrell, J. W. 1995. Decadal trends in the North Atlantic Oscillation: Regional temperatures and precipitation. *Science* **269**, 676–679.
- Huybers, P. and Wunsch, C. 2003. Rectification and precession signals in the climate system. *Geophys. Res. Lett.* **30**, 2011.
- Kaplan, A., Cane, M. A., Kushnir, Y., Clement, A. C., Blumenthal, M. B. et al. 1998. Analyses of global sea surface temperature 1856–1991. *J. Geophys. Res.* **103**, 27 835–27 860.
- Killworth, P. D., Chelton, D. B. and DeZoeke, R. A. 1997. The speed of observed and theoretical long extra-tropical planetary waves. *J. Phys. Oceanogr.* **27**, 1946–1966.
- Latif, M. 1998. Dynamics of interdecadal variability in coupled ocean-atmosphere models. *J. Climate* **11**, 602–624.
- Latif, M. and Barnett, T. P. 1994. Causes of decadal climate variability over the North Pacific and North America. *Science* **266**, 634–637.
- Lau, K.-H. and Shen, P. J. 1988. Annual cycle, quasi-biennial oscillation, and Southern Oscillation in global precipitation. *J. Geophys. Res.* **93**, 10 975–10 988.
- Li, T., Tham, C.-W. and Chang, C.-P. 2001. A coupled air–sea–monsoon oscillator for the tropospheric biennial oscillation. *J. Climate* **14**, 752–764.
- Mann, M. E. and Park, J. 1994. Global-scale modes of surface temperature variability on interannual to century time scales. *J. Geophys. Res.* **99**, 25 819–25 833.
- Mantua, N., Hare, S., Zhang, Y., Wallace, J. M. and Francis, R. 1997. A Pacific interdecadal climate oscillation with impacts on salmon production. *Bull. Amr. Meteorol. Soc.* **78**, 1069–1079.
- Meehl, G. A. 1987. The annual cycle and interannual variability in the tropical Pacific and Indian Ocean region. *Mon. Wea. Rev.* **115**, 27–50.
- Milankovitch, M. 1941. *Kanon der Erdbestrahlung und seine Anwendung auf das Eiszeitproblem*. Spec. Publ. 132, Vol. 33, Sect. Math. Nat. Sci., R. Serb. Acad., Belgrad.
- Mitchell, J. M. 1976. An overview of climatic variability and its causal mechanisms. *Quat. Res.* **6**, 481–494.
- Moore, D. W., Hisard, P., McCreary, J. P., Merle, J., O'Brien, J. J., et al. 1978. Equatorial adjustment in the eastern Atlantic. *Geophys. Res. Lett.* **5**, 637–640.
- Philander, S. G. 1990. *El Nio, La Niña, and the Southern Oscillation*. Academic Press, New York, 293 pp.
- Rogers, J. C. 1984. The association between the North Atlantic Oscillation and the Southern Oscillation in the Northern Hemisphere. *Mon. Wea. Rev.* **112**, 1999–2015.
- Seager, R., Kushnir, Y., Naik, N. H., Cane, N. A. and Miller, J. 2001. Wind-driven shifts in the latitude of the Kuroshio-Oyashio extension and generation of SST anomalies on decadal time scales. *J. Climate* **14**, 4249–4265.
- Terray, L. and Cassou, C. 2002. Tropical Atlantic sea surface temperature forcing of quasi-decadal climate variability over the North Atlantic-European Region. *J. Climate* **15**, 3170–3187.
- Timmermann, A., Latif, M., Voss, R. and Grötzner, A. 1998. Northern Hemispheric interdecadal variability: a coupled air–sea mode. *J. Climate* **11**, 1906–1931.
- Tourre, Y. M., Rajagopalan, B. and Kushnir, Y. 1999. Dominant patterns of climate variability in the Atlantic Ocean region during the last 136 years. *J. Climate* **12**, 2285–2299.
- Tourre, Y. M., Rajagopalan, B., Kushnir, Y., Barlow, M. and White, W. B. 2001. Patterns of coherent decadal and interdecadal climate signals in the Pacific Basin during the 20th century. *Geophys. Res. Lett.* **28**, 2069–2072.
- Trenberth, K. A. and Paolino, D. A. 1980. The Northern Hemisphere sea-level pressure data set: trends, errors and discontinuities. *Mon. Wea. Rev.* **108**, 855–872.
- Vautard, R., Yiou, P. and Ghil, M. 1992. Singular-spectrum analysis: A toolkit for short, noisy chaotic signals. *Physica D* **58**, 95–126.
- von Storch, H. V. and Zwiers, F. W. 1999. *Statistical Analysis in Climate Research*. Cambridge University Press, Cambridge, 484 pp.
- von Storch, H., Bruns, T., Fisher-Bruns, I. and Hasselmann, K. 1988. Principal oscillation pattern analysis of the 30-to 60-day oscillation in a general circulation model equatorial troposphere. *J. Geophys. Res.* **93**, 11 012–11 036.
- White, W. B. and Allan, R. J. 2001. A global quasi-biennial wave in surface temperature and pressure and its decadal modulation from 1900 to 1994. *J. Geophys. Res.* **105**, 26 789–26 803.
- White, W. B. and Cayan, D. R. 2000. A global El Niño-Southern Oscillation wave in surface temperature and pressure and its interdecadal modulation from 1900 to 1997. *J. Geophys. Res.* **105**, 11 223–11 242.
- Xie, S. P. and Tanimoto, Y. 1998. A pan-Atlantic decadal climate oscillation. *Geophys. Res. Lett.* **25**, 2185–2188.
- Zhang, Y., Wallace, J. M. and Battisti, D. S. 1997. ENSO-like interdecadal variability: 1900–93. *J. Climate* **10**, 1004–1020.